

**Explicitly stable fundamental-measure-theory models for classical density functional theory**James F. Lutsko \**Center for Nonlinear Phenomena and Complex Systems CP 231, Université Libre de Bruxelles, Blvd. du Triomphe, 1050 Brussels, Belgium*

(Received 30 September 2020; accepted 30 November 2020; published 17 December 2020)

The derivation of the state of the art tensorial versions of Fundamental Measure Theory (a form of classical Density Functional Theory for hard spheres) is reexamined in the light of the recently introduced concept of global stability of the density functional based on its boundedness [Lutsko and Lam, *Phys. Rev. E* **98**, 012604 (2018)]. It is shown that within the present paradigm, explicit stability of the functional can be achieved only at the cost of giving up accuracy at low densities. It is argued that this is an acceptable trade-off since the main value of DFT lies in the study of dense systems. Explicit calculations for a wide variety of systems show that a proposed explicitly stable functional is competitive in all ways with the popular White Bear models while sharing some of their weaknesses when applied to non-close-packed solids.

DOI: [10.1103/PhysRevE.102.062137](https://doi.org/10.1103/PhysRevE.102.062137)**I. INTRODUCTION**

Classical density functional theory (cDFT) has become an important tool for studying nanoscale phenomena such as the solvation energy of large ions [1], crystallization [2], confinement-induced polymorphism [3], and wetting [4], to name a few. Key to this utility is the ability of cDFT to accurately describe molecular-scale correlations ultimately arising from excluded volume effects. To do this, state of the art cDFT models incorporate as a fundamental building block highly sophisticated functionals for hard spheres that have been developed over the past 30 years. Indeed, the determination of the *exact* functional for hard spheres in one dimension (hard rods) by Percus [5–7] in the 1970s was a key milestone in the development of cDFT and served to inspire the modern class of models known as Fundamental Measure Theory (FMT) [8]. Because of the central role that these play in important applications, the perfection of these models, insofar as possible, remains an important subject of research.

All forms of finite temperature DFT (quantum and classical) are based on fundamental theorems asserting the existence of a functional  $\Lambda[\rho; \phi]$  of the local density  $\rho(\mathbf{r})$  and any one-body fields  $\phi(\mathbf{r})$  having the property that it is uniquely minimized by the equilibrium density distribution for the system,  $\rho_{\text{eq}}(\mathbf{r})$ , and that  $\Lambda[\rho_{\text{eq}}; \phi]$  is the system's (grand-canonical) free energy (for overviews of cDFT see Refs. [9,10]). In general, the dependence on the field is trivial and is separated off by writing  $\Lambda[\rho; \phi] = F[\rho] + \int \rho(\mathbf{r})(\phi(\mathbf{r}) - \mu) d\mathbf{r}$  where the first, field-independent, term  $F$  is called the intrinsic Helmholtz free energy functional and  $\mu$  is the chemical potential. This in turn can be divided into the sum of a (known) ideal-gas term,  $F_{\text{id}}[\rho]$  and an (unknown) excess term  $F_{\text{ex}}[\rho]$  which is the main focus of attention. The FMT model for the excess term was originally developed

by Rosenfeld [8] based on ideas from Scaled Particle Theory. Since then, other approaches to the subject have been explored, and one, so-called dimensional crossover [11,12], has proven particularly fruitful. This starts with a general ansatz for  $F_{\text{ex}}[\rho]$  and then attempts to work out its details by demanding that the theory in, e.g., three dimensions reproduce exact lower-dimensional functionals when suitably restricted. This turns out to lead in a straightforward manner to FMT and was the inspiration for the most sophisticated modern “White Bear” functionals. These give a very good description of inhomogeneous hard-sphere systems including the freezing transition.

While the White Bear functionals (both the original, referred to as WBI [13], and a later, more accurate modification referred to here as WBII [14]) are the best overall models available for three-dimensional systems, they are not without flaws. For example, it has been known for some time that they do not give a very satisfactory description of non-close-packed crystal structures [15]. More importantly, it has recently been demonstrated [16] that they are unstable in the sense that the free energy is unbounded from below leading to the possibility that no global minimum exists. This means that successful applications of these models involve local (metastable) minima, which, while giving physically reasonable results, is in violation of the fundamental theorems of cDFT which say that the equilibrium state must be a global minimum of the free energy functional. The issue is not just philosophical: the local minima can be explored in, e.g., perfect crystals due to the high symmetry, but in more general applications such as those in Refs. [2,3] cited above, a complete lack of symmetry leaves the calculations vulnerable to such unphysical global minima resulting in numerical calculations that blow up. Another conceptual drawback is that to achieve a good quantitative description of dense liquids, the functionals that come out of the dimensional-crossover path are heuristically modified in a way that invalidates the recovery of the low-dimensional results that were their motivation in the first place.

\*jlutsko@ulb.ac.be; <http://www.lutsko.com>

In this paper, I revisit the concept of dimensional crossover while paying particular attention to the question of stability of the functionals. In the next section, it is shown that within the current paradigm of FMT, including the usual but not necessary limits on the complexity of the functionals, explicit global stability can be achieved only by giving up some accuracy at low densities. This seems a fair trade-off as the main utility of cDFT lies in modeling correlations of dense systems for which the low-density accuracy is not so important. The following section presents explicit calculations using an explicitly stable model and shows that it is in most ways comparable in practical accuracy to the most sophisticated White Bear models across a wide range of systems: homogeneous fluid, inhomogeneous fluid near a wall, and various solid structures. The last section summarizes these results and discusses possibilities for further development in this direction.

## II. FUNDAMENTAL MEASURE THEORY AND DIMENSIONAL CROSSOVER

### A. The standard form of FMT

In FMT the excess functional for a single hard-sphere species with radius  $R$  and diameter  $\sigma = 2R$ , is written as

$$F_{\text{ex}}[\rho] = \int \{ \Phi_1[\vec{n}(\mathbf{r}; [\rho])] + \Phi_2[\vec{n}(\mathbf{r}; [\rho])] + \Phi_3[\vec{n}(\mathbf{r}; [\rho])] \} d\mathbf{r}, \quad (1)$$

where  $\rho(\mathbf{r})$  is the local number density and the array of fundamental measures  $\vec{n}$  include the local packing fraction  $\eta(\mathbf{r}; [\rho])$ , and the scalar, vector, and tensor surface measure  $s(\mathbf{r}; [\rho])$ ,  $\mathbf{v}(\mathbf{r}; [\rho])$ , and  $\mathbf{T}(\mathbf{r}; [\rho])$ , respectively:

$$\begin{aligned} \eta(\mathbf{r}; [\rho]) &= \int \Theta(R - r_1) \rho(\mathbf{r} - \mathbf{r}_1) d\mathbf{r}_1, \\ \begin{pmatrix} s(\mathbf{r}; [\rho]) \\ \mathbf{v}(\mathbf{r}; [\rho]) \\ \mathbf{T}(\mathbf{r}; [\rho]) \end{pmatrix} &= \int \begin{pmatrix} 1 \\ \hat{\mathbf{r}}_1 \\ \hat{\mathbf{r}}_1 \hat{\mathbf{r}}_1 \end{pmatrix} \delta(R - r_1) \rho(\mathbf{r} - \mathbf{r}_1) d\mathbf{r}_1. \end{aligned} \quad (2)$$

In the expression for  $F_{\text{ex}}$ , the first contribution

$$\Phi_1(\vec{n}) = -\frac{1}{S_D \sigma^D} s \ln(1 - \eta), \quad (3)$$

where  $S_D$  is the surface area of a sphere with unit diameter in  $D$  dimensions. For  $D = 1$ , this is precisely the exact result of Percus, and, in fact, FMT was developed as part of a general effort at the time to extend this result to higher dimensions. Specializing to three dimensions, the second term is

$$\Phi_2(\vec{n}) = \frac{1}{2\pi\sigma} \frac{s^2 - v^2}{(1 - \eta)}, \quad (4)$$

and the sum  $\Phi_1 + \Phi_2$  has the remarkable property that when applied to a one-dimensional density distribution, e.g.,  $\rho(\mathbf{r}) = \delta(x)\delta(y)\rho(z)$ , it reduces to the exact  $D = 1$  result. Note that such a density corresponds to a 3D system subject to an external field  $\phi_\varepsilon(\mathbf{r})$  which is infinite for  $|x|, |y| > \varepsilon R$  in the limit that  $\varepsilon \rightarrow 0$ : physically, this is a linear tube with radius slightly larger than that of a hard sphere.

### B. Global stability

The overall stability of the functionals demands that they be bounded from below: no density field can give rise to divergent negative  $F_{\text{ex}}[\rho]$  as this would imply that the free energy of the equilibrium system was divergently negative, which is unphysical. However, the structure of FMT leaves this possibility open in that the functions  $\Phi_1$  and  $\Phi_2$  as well as all models for  $\Phi_3$  have numerators that depend on the surface densities divided by denominators that depend on the local packing fraction (a volumetric term). If the numerators are negative at some point  $\mathbf{r}$  for some density field, e.g., if in  $\Phi_2$  one had  $s^2(\mathbf{r}^*; [\rho]) - v^2(\mathbf{r}^*; [\rho]) < 0$  for some  $\rho(\mathbf{r})$ , then one could hold the density constant constant on the sphere  $(\mathbf{r} - \mathbf{r}^*)^2 = R^2$  but increase it inside the sphere with the effect that the numerator remains constant while the denominator,  $1 - \eta(\mathbf{r}^*; [\rho])$ , will eventually become zero giving rise to a divergence. The fact that the functional can diverge at one point does not prove that it is unstable, but it allows for the possibility. In fact, for both  $\Phi_1$  and  $\Phi_2$  this cannot occur: in the former case we have only to note that  $s(\mathbf{r}; [\rho])$  is positive semidefinite, while the non-negativity in the latter case will become apparent below. On the other hand, models for  $\Phi_3$  have long suffered from known instabilities [11] and suspected instabilities (see the discussion in Ref. [16]). Thus, the object here will be to reexamine the reasoning leading to the most useful current models for  $\Phi_3$  and to attempt to modify them so as to impose global stability.

### C. Dimensional crossover

The idea of reproducing exact lower-dimensional results in a higher dimensional system was termed by Rosenfeld and collaborators “dimensional crossover” [11]. One of the only other cases for which exact results are known, besides that of hard rods in one dimension, are the so-called 0D systems consisting of a cavity which is so small that it can hold at most a single hard sphere (see Appendix A for a derivation of the results used here). The minimal example would be a spherical cavity with radius  $R(1 + \varepsilon)$  in the limit that  $\varepsilon \rightarrow 0$  corresponding to a single point. In such a case, the density can take only the form  $\rho_1(\mathbf{r}) = N\delta(\mathbf{r})$  with  $0 \leq N \leq 1$  being the only unknown (its value is determined by the chemical potential). The exact free energy functional is easy to work out,  $F_{\text{ex}}[\rho] = \Phi_0(N[\rho])$ , where  $\Phi_0(x) = (1 - x) \ln(1 - x) - (1 - x)$  and  $N[\rho] = \int \rho(\mathbf{r}) d\mathbf{r}$  is the average number of particles. Other closely related examples are also accessible: for example, two such cavities that do not overlap (a trivial generalization) or, more interestingly, two such cavities which do overlap (see Fig. 1). In the latter case, the combined cavity can still hold only a single hard sphere but the geometry allows a density  $\rho_2(\mathbf{r}) = N_1\delta(\mathbf{r} - \mathbf{s}_1) + N_2\delta(\mathbf{r} - \mathbf{s}_2)$  where  $\mathbf{s}_i$  is the center of the  $i$ th spherical cavity. In this case, the unknown amplitudes must satisfy  $0 \leq N_1 + N_2 \leq 1$ , and the two could be different if, e.g., the external field were different at the two centers. If the two cavities overlap, then one finds that  $F_{\text{ex}}[\rho_2] = \Phi_0(N_1 + N_2)$ , whereas if they do not, then  $F_{\text{ex}}[\rho_2] = \Phi_0(N_1) + \Phi_0(N_2)$ . In the case of three cavities, the results are  $F_{\text{ex}}[\rho_3] = \Phi_0(N_1 + N_2 + N_3)$  if there is a nonzero mutual overlap of all three, it is  $F_{\text{ex}}[\rho_3] = \Phi_0(N_1 + N_2) + \Phi_0(N_3)$  if the first two overlap and neither intersects the

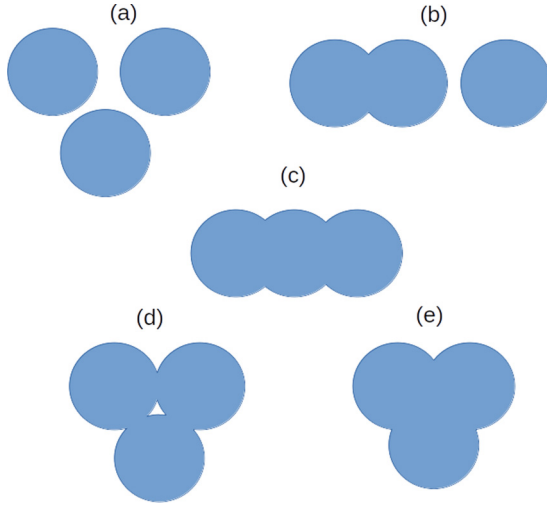


FIG. 1. The different classes of cavities made up of three spherical cavities. Each spherical cavity is just large enough to hold a single hard sphere. The case of two cavities correspond to cases (a) and (b) with one of the detached cavities removed. Cases (c) and (d) cannot be captured by the FMT ansatz.

third volume, and it is  $F_{\text{ex}}[\rho_3] = \Phi_0(N_1) + \Phi_0(N_2) + \Phi_0(N_3)$  if none of them overlap. The results are more complex for the case that cavities 1 and 3 both intersect cavity 2 but do not intersect one another (e.g., a linear chain). This pattern holds for higher numbers of cavities.

To use this information to recover FMT, Rosenfeld and Tarazona [12] proposed that the excess functional be written as a sum of terms,

$$F_{\text{ex}}[\rho] = F_{\text{ex}}^{(1)}[\rho] + F_{\text{ex}}^{(2)}[\rho] + \dots, \quad (5)$$

which are generated by the ansatz

$$\begin{aligned} F_{\text{ex}}^{(1)}[\rho] &= \int d\mathbf{r} \psi_1[\eta(\mathbf{r}; [\rho])] \\ &\times \int d\mathbf{r}_1 \rho(\mathbf{r} - \mathbf{r}_1) \delta(R - r_1) \delta(R - r_2) K_1(\hat{\mathbf{r}}_1), \\ F_{\text{ex}}^{(2)}[\rho] &= \int d\mathbf{r} \psi_2[\eta(\mathbf{r}; [\rho])] \int d\mathbf{r}_1 d\mathbf{r}_2 \rho(\mathbf{r} - \mathbf{r}_1) \\ &\times \rho(\mathbf{r} - \mathbf{r}_2) \delta(R - r_1) \delta(R - r_2) K_2(\hat{\mathbf{r}}_1, \hat{\mathbf{r}}_2), \quad (6) \end{aligned}$$

and so forth. They then evaluated these for various 0D systems: a single cavity, two cavities, etc. It is easy to see that even for the single cavity, the second and all higher contributions will diverge unless the kernels,  $K_n(\hat{\mathbf{r}}_1, \dots, \hat{\mathbf{r}}_n)$

vanish whenever two of the arguments are equal: this is a fundamental stability constraint on the construction of these models since, otherwise, the densities will yield the squares and higher powers of Dirac  $\delta$  functions leading to undefined results (see Appendix B). Since the kernels in the ansatz are scalars, they must be constructed from the scalar products of its arguments, so it is convenient to write them as  $K_1(\hat{\mathbf{r}}_1) = \bar{K}_1(R)$ ,  $K_2(\hat{\mathbf{r}}_1, \hat{\mathbf{r}}_2) = \bar{K}_2(\hat{\mathbf{r}}_1 \cdot \hat{\mathbf{r}}_2; R)$ , etc. Substituting the 0D densities and making use of the stability property of the kernels, one finds that

$$F_{\text{ex}}[\rho_1] = F_{\text{ex}}^{(1)}[\rho_1] = \bar{K}_1 \psi_0(N_1) \frac{\partial}{\partial R} V_D(R), \quad (7)$$

where  $V_D(R)$  is the volume of a sphere of radius  $R$  in  $D$  dimensions and where  $\psi_1(x) = \frac{d}{dx} \psi_0(x) \equiv \psi'_0(x)$ . (See Appendix B for the derivation of this and similar results discussed in this section.) This reproduces the exact result provided  $\psi_0(x) = \Phi_0(x)$  and  $\bar{K}_1 \frac{\partial}{\partial R} V_D(R) = \bar{K}_1 S_D(R) = 1$ , where  $S_D(R)$  is the surface area of the sphere.

For two cavities, after identifying  $\psi_2(x) = \Phi''_0(x)$ , one has that

$$\begin{aligned} F_{\text{ex}}[\rho_2] &= F_{\text{ex}}^{(1)}[\rho_2] + F_{\text{ex}}^{(2)}[\rho_2] \\ &= \Phi_0(N_1 + N_2) + [\Phi_0(N_1 + N_2) - \Phi_0(N_1) \\ &\quad - \Phi_0(N_2)] \{\Delta_2(s_{12}) - 1\}, \quad (8) \end{aligned}$$

where  $\Delta_2(s_{12})$  vanishes if the two cavities do not intersect (thus giving the exact result for this case), and otherwise, in three dimensions, it is

$$\Delta_2(s_{12}) = 1 - \frac{s_{12}}{2R} + \frac{4\pi R^2}{s_{12}} \bar{K}_2 \left( 1 - \frac{s_{12}^2}{2R^2}; R \right). \quad (9)$$

The generalization to any number of dimensions is given in Eq. (B16) of Appendix B. In order to reproduce the exact result, one needs that  $\Delta_2(s_{12}) = 1$  so

$$\bar{K}_2 \left( 1 - \frac{s_{12}^2}{2R^2}; R \right) = \frac{1}{4\pi R} \frac{s_{12}^2}{2R^2} \quad (10)$$

or, equivalently,

$$\bar{K}_2(x; R) = \frac{1}{4\pi R} (1 - x). \quad (11)$$

Before proceeding, it is interesting to see the correspondence between this form of FMT and the more familiar standard form above. Comparing the two, one sees that if  $\bar{K}_n(x_1, x_2, \dots; R)$  is a polynomial of the form  $a_0 + a_1(\hat{\mathbf{r}}_1 \cdot \hat{\mathbf{r}}_2) + a_{11}(\hat{\mathbf{r}}_1 \cdot \hat{\mathbf{r}}_2)^2 + a_{123}(\hat{\mathbf{r}}_1 \cdot \hat{\mathbf{r}}_2)(\hat{\mathbf{r}}_2 \cdot \hat{\mathbf{r}}_3) + \dots$ , etc., then  $F_{\text{ex}}^{(n)}[\rho]$  can be written as

$$F_{\text{ex}}^{(n)}[\rho] = \int \psi_n(\eta(\mathbf{r})) \left\{ \begin{aligned} &a_0 s^n(\mathbf{r}) + a_1 s^{n-2}(\mathbf{r}) v^2(\mathbf{r}) \\ &+ a_{11} s^{n-2}(\mathbf{r}) \text{Tr} T^2(\mathbf{r}) + a_{123} s^{n-3}(\mathbf{r}) \mathbf{v}(\mathbf{r}) \cdot \mathbf{T}(\mathbf{r}) \cdot \mathbf{v}(\mathbf{r}) \dots \end{aligned} \right\} d\mathbf{r} \quad (12)$$

so that in particular with the kernels given above,

$$F_{\text{ex}}^{(1)}[\rho_2] + F_{\text{ex}}^{(2)}[\rho_2] = \int \left\{ \frac{1}{4\pi R^2} s(\mathbf{r}) \ln [1 - \eta(\mathbf{r})] + \frac{1}{4\pi R} \frac{s^2(\mathbf{r}) - v^2(\mathbf{r})}{[1 - \eta(\mathbf{r})]} \right\} d\mathbf{r}, \quad (13)$$

which are the first two terms of Rosenfeld's functional in three dimensions. One sees that it is possible to write the free energy

functional in the standard FMT formulation only if the kernels are polynomial functions of their arguments.

To describe three cavities, let  $V_{ij}$  be the volume of intersection of spheres of radii  $R_i$  and  $R_j$  with centers  $\mathbf{s}_i$  and  $\mathbf{s}_j$  and let  $V_{ijk}$  be the volume of mutual intersection for three such spheres. Then, for  $V_{12} = V_{13} = V_{23} = 0$  [case (a) in Fig. 1], the exact result is  $F_{\text{ex}}[\rho_3] = \Phi_0(N_1) + \Phi_0(N_2) + \Phi_0(N_3)$ , and this is reproduced by the FMT ansatz, provided the kernels satisfy the stability condition. For  $V_{12} \neq 0, V_{13} = V_{23} = 0$  [case (b)] both give  $F_{\text{ex}}[\rho_3] = \Phi_0(N_1 + N_2) + \Phi_0(N_3)$ . The cases  $V_{12} \neq 0, V_{13} \neq 0, V_{23} = 0$  [case (c)] and  $V_{12} \neq 0, V_{13} \neq 0, V_{23} \neq 0, V_{123} = 0$  [case

(d)] give rise to more complicated exact results, while FMT gives  $\Phi_0(N_1 + N_2) + \Phi_0(N_1 + N_3) - \Phi_0(N_1)$  in the first case and  $\Phi_0(N_1 + N_2) + \Phi_0(N_1 + N_3) + \Phi_0(N_2 + N_3) - \Phi_0(N_1) - \Phi_0(N_2) - \Phi_0(N_3)$  in the second case, neither of which is correct. Furthermore, there is clearly no freedom within this ansatz to capture the correct results. Rosenfeld and Tarazona label these “lost cases” as they simply cannot be described within this framework. The final possibility,  $V_{123} \neq 0$  [case (e)] yields the expected exact result  $\Phi_0(N_1 + N_2 + N_3)$ , and the ansatz gives, after identifying  $\psi_3(x) = \Phi_0'''(x)$ ,

$$F_{\text{ex}}^{(1)}[\rho_2] + F_{\text{ex}}^{(2)}[\rho_2] + F_{\text{ex}}^{(3)}[\rho_2] = \Phi_0(N_1 + N_2 + N_3) + \left\{ \sum_i \Phi_0(N_i) - \sum_{i<j} \Phi_0(N_i + N_j) + \Phi_0(N) \right\} \{ \Delta_3(s_{12}, s_{13}, s_{23}) - 1 \}, \tag{14}$$

where  $\Delta_3(s_{12}, s_{13}, s_{23})$  vanishes if  $V_{123} = 0$  and otherwise it is

$$\Delta_3(s_{12}, s_{13}, s_{23}) = \lim_{R_1, R_2, R_3 \rightarrow R} \left\{ \bar{K}_1 \sum_{i=1}^3 \frac{\partial}{\partial R_i} V_{123} + \frac{1}{4\pi R} \sum_{i=1}^3 \sum_{j=i+1}^3 \frac{s_{ij}^2}{R^2} \frac{\partial^2}{\partial R_i \partial R_j} V_{123} + 6\bar{K}_3(\dots) \frac{\partial^3}{\partial R_1 \partial R_2 \partial R_3} V_{123} \right\}, \tag{15}$$

where the arguments of  $\bar{K}_3$  have been suppressed for clarity. Reproduction of the exact result demands that  $\Delta_3 = 1$  thus determining  $\bar{K}_3$ . The various volume derivatives can be worked out, but they are quite complicated, involving square roots, inverse trigonometric functions, and many different cases: the exact expression can clearly not be written as a polynomial, except perhaps as an infinite expansion. For example, for the most symmetric case  $s_{12} = s_{13} = s_{23} = D$ , it simplifies to

$$\bar{K}_3(x, x, x) = \frac{1}{48} (1-x) \sqrt{1+2x} \left( 1 - \frac{6}{\pi} \arcsin \frac{x}{1+x} \right), \tag{16}$$

which we can confirm vanishes at  $x = 1$ , as demanded by the stability condition.

In summary, the dimensional crossover program has successfully generated the first and second contributions to the excess free energy functional of Rosenfeld’s FMT. It is known that the sum of these two terms also reproduces the exact 1D functional (the Percus functional) when the density is suitably restricted, and it is easy to show that the higher-order terms do not contribute to this limit provided they satisfy the stability condition (see Appendix C). However, for three cavities, only the simplest cases of at least one completely disjoint sphere

are reproduced correctly (and these cases do not involve  $K_3$ ). Two classes of configurations are *a priori* inaccessible to the ansatz while the third, involving three cavities that have a nonzero mutual intersection, can be recovered but the kernel is a complicated, nonpolynomial function of its arguments. The latter fact means that it cannot be expressed in terms of a finite number of fundamental measures. From a practical point of view, it is imperative to have such a formulation in terms of fundamental measures expressed as convolutions that they can be evaluated efficiently. This impasse suggests that we ask what properties could be preserved by an “acceptable” kernel. Evidently, it must be a polynomial function of its arguments, and if we want to restrict the possibilities to those that generate functionals involving only the fundamental measures already discussed, then the most general form possible, taking account of symmetry, is

$$\bar{K}_3(x, y, z) = a + b(x + y + z) + c(x^2 + y^2 + z^2) + d(xy + xz + yz) + exyz. \tag{17}$$

The stability condition demands that  $\bar{K}_3(x, x, 1)$  vanish, so

$$0 = (a + b + c) + (2b + 2d)x + (2c + d + e)x^2, \tag{18}$$

and since  $x$  can vary freely, the various coefficient must vanish leaving, after renaming the remaining constants,

$$\bar{K}_3(x, y, z) = \frac{1}{24\pi} A(1-x)(1-y)(1-z) + \frac{1}{24\pi} B(1-x^2-y^2-z^2+2xyz),$$

which, in terms of the vectors, can be written as

$$K_3(\hat{\mathbf{r}}_1, \hat{\mathbf{r}}_2, \hat{\mathbf{r}}_3) = \frac{1}{24\pi} A(1 - \hat{\mathbf{r}}_1 \cdot \hat{\mathbf{r}}_2)(1 - \hat{\mathbf{r}}_1 \cdot \hat{\mathbf{r}}_3)(1 - \hat{\mathbf{r}}_2 \cdot \hat{\mathbf{r}}_3) + \frac{1}{24\pi} B|\hat{\mathbf{r}}_1 \cdot (\hat{\mathbf{r}}_2 \times \hat{\mathbf{r}}_3)|^2. \tag{19}$$

TABLE I. The  $n$ th virial coefficient in the PY approximation, the result of esFMT for arbitrary values of the coefficients  $A, B$  and where  $C = \frac{1}{3}(8A + 2B - 9)$  and the exact values [18].

$n$	$B_n^{(\text{PY})}$	$B_n^{(\text{esFMT})}$	$B_n^{(\text{exact})}$
2	4	4	4
3	10	10+C	10
4	19	19+3C	18.36
5	31	31+6C	28.22
6	46	46+10C	39.82
7	64	64+15C	53.34

Thus, the only practical question is how to determine the constants,  $A$  and  $B$ . The original FMT of Rosenfeld is recovered by taking  $A = 9/8, B = 0$  and keeping only the lowest-order (linear) terms involving the scalar products while the tensor version of Tarazona corresponds to  $A = -B = 3/2$ . Note that the coefficients of the two constants are obviously non-negative so that  $A, B \geq 0$  automatically ensures stability of the resulting functional. Indeed, since  $\bar{K}_3(-0.5, -0.5, -0.5) = \frac{9}{64\pi}A$  the kernel can only be non-negative for all arguments if  $A \geq 0$ . Similarly,  $\bar{K}_3(1 - \varepsilon, 1 - \varepsilon, 1 - \varepsilon) = \frac{1}{24\pi}\varepsilon^2[\varepsilon A + (3 - 2\varepsilon)B]$  so non-negativity for vanishingly small  $\varepsilon$  also demands that  $B \geq 0$ . The fact that the existing tensor functionals are well outside these limits is most likely the source of their instability. In

the following, the class of theories discussed here with coefficients  $A, B > 0$  will be called “explicitly stable FMT” or “esFMT( $A, B$ ).” The qualification is due to the fact that it is possible that negative coefficients could also yield a stable (in the sense of bounded from below) theory, but this is not obvious.

### III. PROPERTIES OF EXPLICITLY STABLE FUNCTIONALS

In summary, the class of “explicitly” stable functionals consistent with dimensional crossover and involving only measures up to the second-order tensor are  $F_{\text{ex}}[\rho] = F_{\text{ex}}^{(1)}[\rho] + F_{\text{ex}}^{(2)}[\rho] + F_{\text{ex}}^{(3)}[\rho]$  with the third contribution having the form

$$F_{\text{ex}}^{(3)}[\rho] = \frac{1}{24\pi} \int \frac{1}{[1 - \eta(\mathbf{r})]^2} \left\{ \begin{array}{l} (A + B)s^3(\mathbf{r}) - 3As(\mathbf{r})v^2(\mathbf{r}) + 3A\mathbf{v}(\mathbf{r}) \cdot \mathbf{T}(\mathbf{r}) \cdot \mathbf{v}(\mathbf{r}) \\ -3Bs(\mathbf{r}) \text{Tr } \mathbf{T}^2(\mathbf{r}) + (2B - A) \text{Tr } \mathbf{T}^3(\mathbf{r}) \end{array} \right\} d\mathbf{r} \quad (20)$$

with  $A, B \geq 0$ . This expression, written in the usual language of FMT, is obtained by substituting Eq. (19) into the three-body term generated by the ansatz of Eq. (6) and then using the definitions of the fundamental measures given in Eq. (2). The original proposal of Tarazona is not in this class as it requires  $A = -B = \frac{3}{2}$ . As shown below, any combination  $A + B/4 = 1$  gives the Percus-Yevik (PY) equation of state, but the PY direct correlation function (dcf) can be obtained only via the Tarazona model (which, indeed, was the reason for its form). These “explicitly stable” models give finite results for any of the combinations of OD cavities and are positive semidefinite (hence implying that the free energy is bounded from below for any density field). Having defined, as precisely as possible, the class of explicitly stable models, this section is devoted to investigating the results of various choices for the constants  $A$  and  $B$ .

The next subsection deals with the properties of the homogeneous fluid, the following with the inhomogeneous fluid, and the remainder with the solid phase. Calculations on inhomogeneous systems were performed by discretizing the density field on a cubic lattice with spacing  $\Delta$ , which is typically much smaller than a hard-sphere radius. Details of the calculations (using analytic representations of the fundamental measures and a consistent real-space scheme to evaluate the convolutions) have been given in a recent publication [17]. This discretized density is used to evaluate the functional  $\Lambda[\rho]$ , which is then minimized with respect to the density in a scheme we refer to as “full minimization” since, beyond the discretization, there are no constraints on the calculations. For the solid phases, some calculations were also performed using an approximate “constrained” scheme whereby the density is written as a sum of Gaussians,

$$\rho(\mathbf{r}) = (1 - c) \sum_{\mathbf{R}} \left( \frac{\alpha}{\pi} \right)^{3/2} \exp[-\alpha(\mathbf{r} - \mathbf{R})^2], \quad (21)$$

where  $0 \leq c < 1$  is the vacancy concentration, the sum is over the Bravais lattice sites, and the parameter  $\alpha$  controls the width of the Gaussians. For a face-centered cubic (FCC)

or body-centered cubic (BCC) lattice, this represents a solid with lattice density  $\rho_{\text{latt}} = 4/a^3$  or  $2/a^3$ , respectively, where  $a$  is the cubic lattice constant. In both cases, the average number density (e.g., the integral of the density over all space divided by the volume) is  $\bar{\rho} = (1 - c)\rho_{\text{latt}}$ . By converting this sum to Fourier space it is easy to see that  $\alpha = 0$  corresponds to a uniform density of  $\bar{\rho}$  so that varying  $\alpha$  allows one to go smoothly from the fluid to the solid state. In our Gaussian calculations, the vacancy concentration is generally fixed to some small value, e.g.,  $c = 10^{-4}$ , and we minimize with respect to  $\alpha$ . Generally, most properties of the solid are insensitive to the precise value of  $c$ , but one could of course minimize with respect to this parameter as well. Note that in general, the vacancy concentration is calculated as  $c = (N_{\text{latt}} - N[\rho])/N_{\text{latt}}$  where  $N_{\text{latt}}$  is the number of lattice sites in the system (i.e., 4 per cubic unit cell for FCC and 2 for BCC). Finally, a standard measure of the widths of the distributions is the Lindemann parameter defined as the root-mean-square displacement divided by the nearest-neighbor distance.

#### A. Properties the homogeneous fluid

Keeping the constants arbitrary for the moment, the resulting equation of state for the homogeneous fluid ( $\rho(\mathbf{r}) \rightarrow \rho$  and  $\eta(\mathbf{r}) \rightarrow \eta = \pi\rho\sigma^3/6$ ) is

$$\frac{\beta P}{\rho} \equiv Z(A, B) = Z^{PY} + \left[ \frac{2}{3}(4A + B) - 3 \right] \frac{\eta^2}{(1 - \eta)^3}, \quad (22)$$

where the Percus-Yevik compressibility factor is

$$Z^{PY} = \frac{1 + \eta + \eta^2}{(1 - \eta)^3}, \quad (23)$$

and we recall that both the Rosenfeld and Tarazona functionals reproduce PY. The first several terms of the virial expansion are given in Table I. The direct correlation function for the homogeneous liquid is calculated from the exact relation [10]  $c(\mathbf{r}_1, \mathbf{r}_2; [\rho]) = -\delta^2 \beta F_{\text{ex}}[\rho] / \delta \rho(\mathbf{r}_1) \delta \rho(\mathbf{r}_2)$  evaluated

at constant density yielding

$$c(r = \sigma x; A, B) = c^{PY}(r) + \left\{ \begin{array}{l} -\frac{1}{2} \frac{\eta}{(1-\eta)^2} x [2(A+B)x^2 + 3 - 2B - 4A] \\ + (8A + 2B - 9) \frac{\eta^2}{(1-\eta)^3} (1-x) \left[ 1 + \frac{1}{2} \frac{\eta}{1-\eta} (1-x)(2+x) \right] \end{array} \right\} \Theta(1-x). \quad (24)$$

To recover the PY equation of state requires that  $4A + B = \frac{9}{2}$  in which case the PY dcf is also recovered with  $A = -B$ , which is again Tarazona’s model.

So, if one wishes to be sure that the resulting functional is stable for any density distribution, and therefore demands that  $A, B \geq 0$ , then it is impossible to reproduce the PY direct correlation function. In any case, this is not an exact result, so there is no particular requirement to do so (and, in fact, the White Bear functionals do not). However, since PY is exact up to second order in the density, a difference from the PY expression of first order in the density also means that one does not recover the exact dcf up to first order, which may be more disturbing but, unavoidable, if the functional is to be explicitly stable. A reasonable result is achieved if one takes, e.g., for simplicity,  $A = 1$  and  $B = 0$ , which means that  $C = -\frac{1}{3}$ . This creates a small error at order  $\eta^2$  but improves the virial expansion at higher order. For example, it gives  $B_3 = 9\frac{2}{3}$  and  $B_7 = 59$  compared to the exact values of 10 and 53.34, respectively and the compressibility factor is generally improved by this choice relative to PY; see Fig. 2. Figure 3 shows the dcf for  $(A, B) = (1, 0)$  and  $(0, 4)$ , both corresponding to  $C = -\frac{1}{3}$ , compared to PY, the dcf generated by the WBI approximation and simulation data. At small values of  $r$ , the dcf generated by the stable FMT is actually closer to simulation than that of WBI or the PY result. At the largest value,  $r = \sigma$ , the esFMT is not as close but the deviations are not very large.

**B. Fluid near a wall**

As a first example of an inhomogeneous system, the structure of a fluid in contact with a wall is shown in Figs. 4 and 5 for bulk densities  $\rho\sigma^3 = 0.813$  and  $0.9135$  corresponding to packing fractions of 0.426 and 0.478, respectively. The

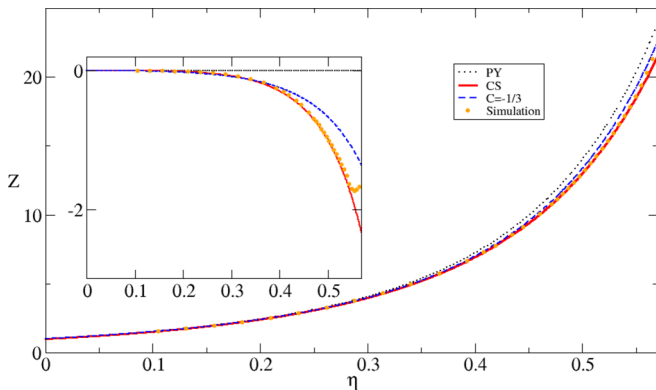


FIG. 2. Compressibility factor  $Z = \beta P / \rho$  for the homogeneous liquid as a function of density as predicted by the Percus-Yevik (PY) and Carnahan-Starling (CS) equations of state, Eq. (22) with  $C = -1/3$ , and simulation data reported in Ref. [19]. The inset shows the difference of the various quantities from the PY prediction.

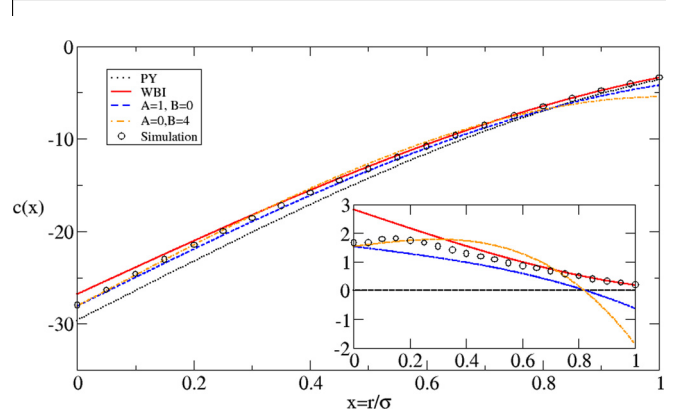


FIG. 3. Direct correlation function for the uniform hard-sphere fluid at density  $\rho\sigma^3 = 0.8$ , or  $\eta = 0.4189$ , as predicted by the Percus-Yevik theory, the WBI model, the esFMT with two different choices of parameters (which give the same equation of state), and simulation data reported in Ref. [20]. The inset shows the differences from the PY result. Note that the exact dcf is also nonzero outside the hard-core, but none of the theories considered here allow for this.

esFMT agrees quite closely with the WBI and WBII functionals, and all are in reasonable agreement with simulation at the lower density but show similar deviations at the higher density. This is due to the fact that all FMTs obey the wall theorem [10], which says that the density of a fluid of hard spheres at the point of contact with a hard wall will be  $\beta P$ , so, since the esFMT equation of state is somewhat different than that of the WB models, the contact density necessarily differs also. In any case, the differences between all of these models is quite small.

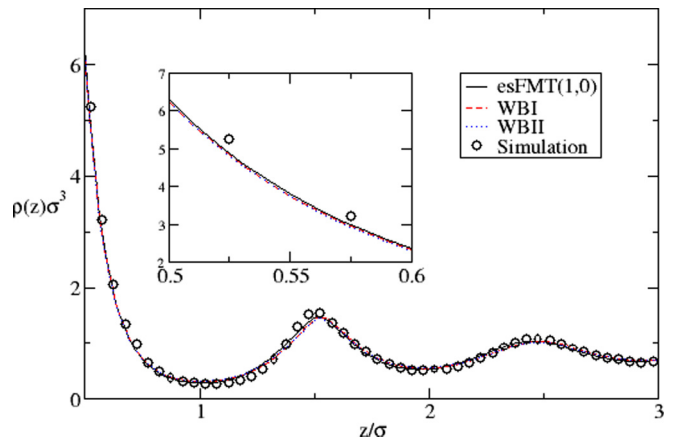


FIG. 4. Fluid structure near a wall with bulk density  $\rho\sigma^3 = 0.813$ , or  $\eta = 0.426$ , for the WBII model and the esFMT(1,0) model. All calculations were performed on a grid of  $1 \times 1 \times 10000$  points with spacing  $\Delta = 0.01\sigma$ . The simulation results are from Ref. [21]. The inset shows the slight differences at the point of contact with the wall.

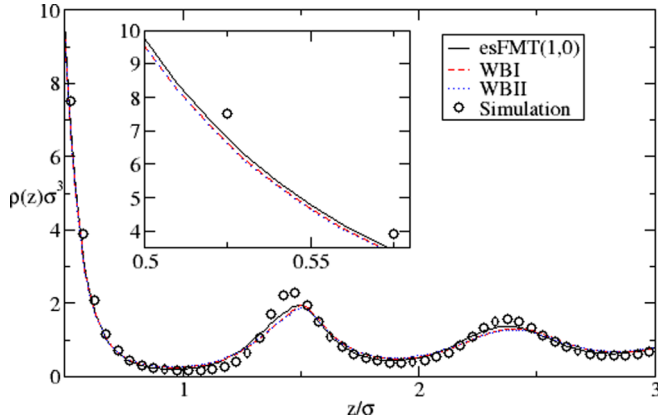


FIG. 5. As in Fig. 4 for a density of  $\rho\sigma^3 = 0.9135$ , or  $\eta = 0.478$ .

### C. Freezing transition

The freezing of hard spheres (into an FCC solid) has long served as a benchmark problem for the development of new model functionals. In the framework of cDFT the procedure is conceptually straightforward: one must minimize the density functional at fixed chemical potential (i.e., in the grand canonical ensemble) to find the metastable states: typically, one constant density (fluid) state and a solid state with the density localized at the Bravais lattice sites. The state with the smallest free energy is thermodynamically favored, and at some chemical potential, the free energies of the two states are equal thus determining the freezing transition.

In early work, the density was almost always modeled as a sum of Gaussians (or, sometimes, distorted Gaussians) centered at the FCC lattice sites. In the simplest case, the Gaussians have a fixed normalization (less than or equal to one) and the free energy functional reduces to a function of two parameters, the width of the Gaussians and the FCC lattice constant. At little more expense, one can allow the normalization of the Gaussians to vary as well yielding a function of three parameters. In both cases, the function must then be minimized to determine the equilibrium state. It happens that Gaussians with infinite width give a uniform density which corresponds to the homogeneous fluid, so by varying the width, one passes from the fluid to the solid thus allowing both to be described in the same framework. More recent

applications (including the present work) simply discretize the density on a grid (with computational unit cells much smaller than the FCC unit cell), and one then minimizes with no constraints. These calculations are usually performed in two steps: minimization at constant lattice parameter, and then minimization over the lattice parameters. Further details of the implementation used in this work can be found in [17]. Table II shows the results obtained for the freezing transition using the esFMT, the original Tarazona theory (corresponding to  $A = -B = 3/2$ ), the WBI and WBII theories, and simulation results.

The explicitly stable model with  $A = 1, B = 0$  gives results quite similar to WBI: this may be a little surprising since the quality of the prediction of freezing is tied to the accuracy of the fluid equation of state, and the Carnahan-Starling equation of state that is built into WBI is better than that of esFMT(1,0). In any case, as for the homogeneous fluid, the esFMT seems to perform almost as well as the state of the art. In particular, Table II includes results for a nontensorial model that is also positive semidefinite, but which does not correctly describe multiple 0D cavities (the model discussed in Ref. [16] and referred to as “mRSLT”). Despite incorporating the same equation of state as WBI, it performs much worse in predicting hard-sphere freezing.

Finally, the table also gives the vacancy concentration at freezing (calculated for a unit cell of the FCC lattice as  $c = \frac{4-N}{V}$  with  $N$  the total number of molecules in the cell and  $V$  its volume). These numbers are not necessarily very accurate since the grid spacing ( $\Delta = 0.025\sigma$ ) does not allow for a very accurate representation of the density peaks when they are too sharp, but it is consistent with calculations on finer grids. Given that the values determined from simulation for densities near freezing are on the order of  $10^{-4}$ , the important point is that, as noted previously [16], the WB models give typical values about an order of magnitude smaller than simulation while the esFMT seems to improve on this somewhat.

### D. Solid structure and thermodynamics

Figure 6 shows the pressure factor for the FCC solid as a function of packing fraction for the esFMT(1,0) model compared to simulation. The calculations were performed using full minimization with spacings  $\Delta = 0.025\sigma$  and  $0.0125\sigma$  as well as minimization of Gaussian profiles on this and finer

TABLE II. Freezing parameters as calculated using several different FMT models and simulation results. All calculations were performed using full minimization on a lattice with spacing  $\Delta = 0.025\sigma$  except for the Tarazona model, which was estimated using Gaussian profiles. The Lindemann parameter is the square root of the mean-squared displacement divided by the nearest-neighbor distance. The simulation results are from Fortini and Dijkstra [22], except the Lindemann parameter taken from Ref. [20] and the vacancy concentration, which is an estimate based on Ref. [23]. For the esFMT, calculations on a lattice with spacing  $\Delta = 0.0125\sigma$  yield virtually identical results. The table also includes results based on a more heuristic approach to explicit stability called “mRSLT” in Ref. [16].

Source	$\eta_{\text{liq}}$	$\eta_{\text{solid}}$	$\beta P\sigma^3$	$\beta\mu$	Lindemann parameter	Vacancy concentration
WBI	0.491	0.534	11.50	16.0	0.138	$-7 \times 10^{-6}$
WBII	0.498	0.544	12.17	16.70	0.122	$4 \times 10^{-5}$
Tarazona	0.472	0.518	10.04	14.56	0.149	—
esFMT(1,0)	0.486	0.533	11.28	15.8	0.141	$6 \times 10^{-4}$
mRSLT	0.514	0.547	14.14	18.73	0.133	$-2 \times 10^{-4}$
Simulation	0.4915(5)	0.5428(5)	11.57(10)	16.08(10)	0.126	$1.4 \times 10^{-4}$

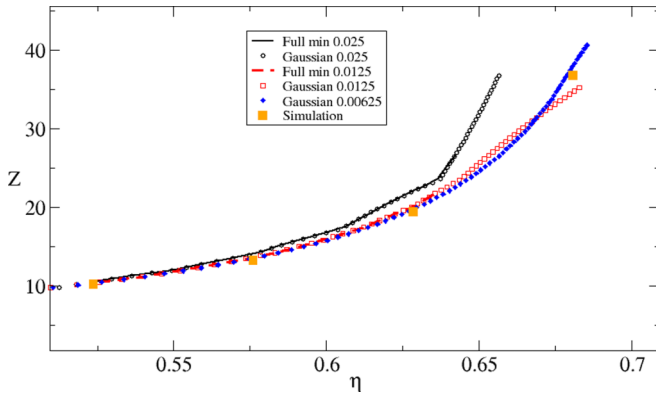


FIG. 6. Pressure factor as determined from the esFMT(1,0) theory using full minimization with a computational lattice spacing of  $\Delta = 0.025\sigma$  and minimization of Gaussians with spacings  $\Delta = 0.025\sigma$ ,  $0.0125\sigma$ , and  $0.00625\sigma$ . Simulation results are taken from Bannerman *et al.* [24]. The results of full minimization and of the Gaussian approximation are indistinguishable.

lattices. Little difference is seen between the full minimization and the Gaussian model. In each case, the results are in good agreement with simulation up to some maximum packing fraction at which point the solid peaks become so narrow that that the lattice is no longer able to accurately represent them.

Figure 7 shows a similar comparison for the ratio of the root-mean-squared displacement divided by the nearest-neighbor distance, i.e., the Lindemann parameter. Again, all of the calculations are in good agreement with simulation up to the limits imposed by the lattice.

The vacancy concentration is shown in Fig. 8. It is a very small quantity compared to the density and so is quite sensitive to numerical noise, but the values obtained from the esFMT(1,0) model are again in reasonable agreement with simulation.

**E. The BCC crystal**

One of the weaknesses of FMT is the description of non-FCC crystals. Older forms of cDFT never gave very good descriptions of the BCC structure at high density: in

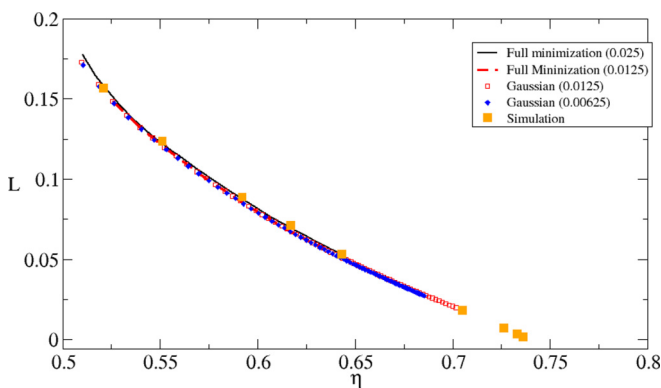


FIG. 7. Same as Fig. 6 but showing the Lindemann parameter. The simulation results are from Alder and Young [20]. Again, the constrained and unconstrained results are virtually identical.

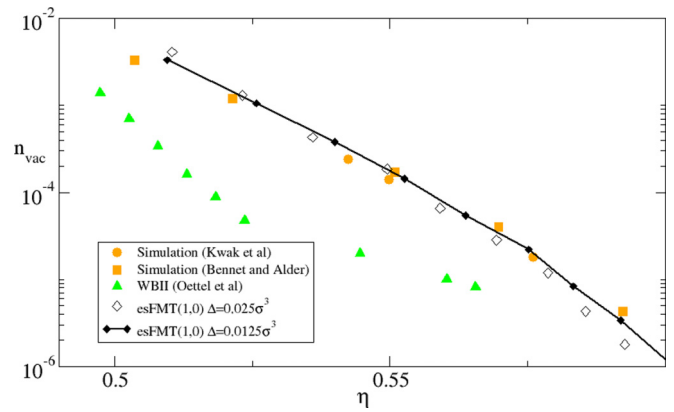


FIG. 8. The vacancy concentration as a function of density as determined by full minimization of esFMT(1,0) with lattice spacing  $\Delta = 0.0125\sigma$  and  $0.00625\sigma$ , the results reported by Oettel *et al.* [25] and from simulations by Kwak *et al.* [26] and Bennet and Alder [23].

particular, the Lindemann parameter decreased only slightly as density increased and eventually began to increase with increasing density, which is very unphysical behavior(see, e.g., Ref. [27]). One of the impressive accomplishments of the original tensor version of FMT is that it predicts that the Lindemann parameter of the BCC crystal goes to zero at BCC close packing just as it should [28]. However, upon further examination [15], it was found that this was preceded by a similarly unphysical behavior and that in fact that there are really two BCC structures: one that shows the same unphysical behavior as the older theories gave, and one that gives the new, more physical behavior. Furthermore, the unphysical structure has the lower free energy for packing fractions below about  $\eta = 0.6$ . The White Bear theories were even worse with the unphysical structure always being the more stable of the two. So it is interesting to ask whether the esFMT does any better or worse.

In Fig. 9 the free energy of the BCC structure calculated in the Gaussian approximations is shown as a function of the Gaussian parameter  $\alpha$  for several different densities. The liquid state corresponds to  $\alpha = 0$ , and one sees that there is indeed a solid-like minimum as well but at a value that is relatively low compared to the FCC solid. This is not surprising since the BCC structure is not close-packed, and so the molecules are expected to have more room to move. However, it is apparent from the figure that this minimum does not really increase with increasing density and that at high densities, a second minimum appears at much higher values of  $\alpha$ . This second minimum does increase quickly with density near close packing as one would expect, and in all cases, it is very shallow leaving the low- $\alpha$  minimum as the thermodynamically more stable of the two. This behavior is very similar to that of the WBI theory and shows that, as in other forms of FMT, the stable theory does not give a particularly physical description of the BCC state.

The figure also shows results using WBI and Tarazona’s original tensor model. The similarity between esFMT(1,0) and WBI is again evident with the curves being nearly indistinguishable. This is not the case with Tarazona’s model, which shows a considerably higher first barrier and

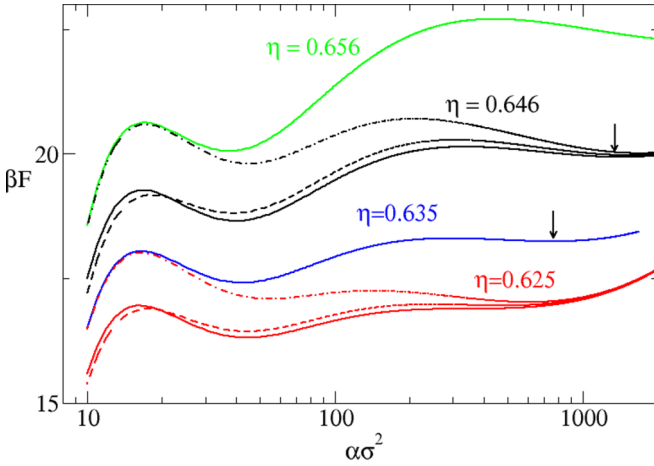


FIG. 9. Free energy divided by temperature as a function of the Gaussian parameter,  $\alpha$ , for the BCC crystal at several different densities as determined using the esFMT(1,0) theory. The minima, marked with arrows, correspond to metastable crystal states for the esFMT(1,0) model. The dashed lines are the WBI results, and the dot-dash lines are from Tarazona's original tensor model at  $\eta = 0.625$  and  $0.646$ .

minimum than the other two, whereas the second minimum is quite similar in position to that of the the other two theories. Recall that Tarazona's model gives the PY equation of state for the homogeneous fluid (corresponding to  $\alpha = 0$ ), whereas WBI reproduces Carnahan-Starling and the esFMT(1,0) gives something close to Carnahan-Starling. For the homogeneous fluid at  $\eta = 0.625$ , this means that Tarazona gives a free energy divided by temperature that is approximately 0.84 higher than the other two, and this corresponds roughly to the differences in the height of the first peaks and first minima of the free energy curves, while for  $\eta = 0.655$  the difference is 1.1, which again is similar to the differences of the first peaks and first minima. It therefore seems that the main difference between the various tensor models in the case of the BCC system is that the Tarazona model goes to the less accurate and somewhat higher PY free energy at  $\alpha = 0$ , and this continues to cause an increase in the free energies at the low values of  $\alpha$  at which the first minimum occurs, whereas it is forgotten at the high values of  $\alpha$  where the second minimum occurs, and all three models give very similar results.

One conclusion of these strange features is that the current functionals, including the class proposed here, are deficient in some way. Another is that the anomalous features are real and arise out of the instability of the hard-sphere BCC system. It has recently been shown that a similar, but distinct, crystalline structure (the cI16 lattice) is metastable and that this has generally not been seen in DFT calculations because it requires a much larger unit cell (corresponding to a  $2 \times 2 \times 2$  BCC system) [29,30]. It will be interesting in the future to investigate this possibility using unconstrained calculations that do not depend on a predefined lattice structure.

#### IV. CONCLUSION

In this paper, the arguments leading to the most popular form of FMT, namely, the White Bear functionals, have been reexamined in light of the demand for global stability of the

functionals. The requirement that the functionals reproduce the known exact results for a simple spherical cavity just large enough to contain a single hard sphere (e.g., a primitive 0D cavity), for any combination of two such cavities, for certain examples of three such cavities, and for a one-dimensional density distribution provide strong constraints on the possible model functionals. Using the ansatz of Tarazona and Rosenfeld, as well as demanding computational practicality (e.g., limiting the complexity of the three-body kernel so that it is representable using scalar, vector, and second-order tensors measures only), leads to a two-parameter class of possible functionals. If one further imposes that the first-order density correction to the dcf of the homogeneous fluid is recovered, the parameters are fixed to those originally suggested by Tarazona [28] and that form the basis of the White Bear functionals. The main observation of this work is that such a choice cannot be proven to be globally stable (and, indeed, as noted above there is strong evidence that it is not [16]), and so alternatives were considered which do give global stability at the cost of less accuracy at low density.

The proposed functional, labeled esFMT(1,0), is not only stable but seems comparable to the WBI model in most numerical tests: it gives an equation of state for the homogeneous system which is better than PY, if not quite as accurate as Carnahan-Starling, it performs similarly for fluids near a wall, and the solid phase properties are all comparable to WBI. The main exception to the last statement is in the vacancy concentration of the FCC solid where the proposed model is in good agreement with simulation—better than WBII and much better than WBI. This is, however, most likely a chance result and may not hold any real significance in terms of the quality of the model. Like the WB models, the explicitly stable FMT shows somewhat unphysical behavior for the BCC phase, and so this remains an overall weakness of the FMT approach. Aside from the important issue of global stability, perhaps the biggest conceptual virtue of the esFMT is that it achieves this positive comparison with WB without introducing the heuristics of the WB models (which explicitly build in the CS equation of state). One could also note that a practical consequence of this is that the analytic form is somewhat simpler than that of WB. Overall, the esFMT(1,0) model seems to be adequate for any current application.

In an ideal world, one would of course prefer to recover the low-density limits as well, but this would seem to only be possible if the model were extended to higher tensorial order—something which is not impossible but which will require further work. One would also like to have a more robust criterion for the selection of the remaining parameters, and here it may be that something could be done using the ideas of Santos [31] concerning thermodynamic consistency of mixtures, which have yet to be fully incorporated into FMT.

#### ACKNOWLEDGMENTS

This work of J.F.L. was supported by the European Space Agency (ESA) and the Belgian Federal Science Policy Office (BELSPO) in the framework of the PRODEX Programme, Contract No. ESA AO-2004-070.

**APPENDIX A: EXACT RESULTS FOR A 0D CAVITY**

To illustrate the calculations used to determine the free energy of configurations of 0D cavities, consider first a cavity  $S$  in  $D$  dimensions which is large enough to hold a single hard sphere but not large enough to contain more than one without overlap. The grand partition function is

$$\Xi[\vec{\phi}] = 1 + \Lambda^{-D} \int_S \exp[-\beta(\phi(\mathbf{q}_1) - \mu)] d\mathbf{q}_1, \tag{A1}$$

where  $\Lambda$  is the thermal wavelength,  $\phi(\mathbf{r})$  is the external field (which is infinite outside the cavity but arbitrary within), and  $\mu$  is the chemical potential. There are only two terms, corresponding to zero and one particles. The grand canonical free energy is  $\Omega[\phi] = -k_B T \ln \Xi[\vec{\phi}]$ , and the local density is given by the standard relation

$$n(\mathbf{r}) = -\frac{\delta\Omega[\phi]}{\delta\phi(\mathbf{r})} = \frac{\Lambda^{-D} \exp\{-\beta[\phi(\mathbf{r}) - \mu]\}}{1 + \Lambda^{-D} \int_S \exp\{-\beta[\phi(\mathbf{q}_1) - \mu]\} d\mathbf{q}_1}. \tag{A2}$$

This can be inverted to give the field in terms of the density

$$\exp\{-\beta[\phi(\mathbf{r}) - \mu]\} = \frac{\Lambda^D n(\mathbf{r})}{1 - \int_V n(\mathbf{q}) d\mathbf{q}} \equiv \frac{\Lambda^D n(\mathbf{r})}{1 - N[n]}, \tag{A3}$$

where the equivalence identifies the average number of particles in the cavity, which, by hypothesis, is  $0 \leq N[n] \leq 1$ . Recall that the cDFT functional evaluated at the equilibrium density  $n[\phi]$  gives the grand canonical free energy,  $\Omega[\phi] = \Lambda[n[\phi]; \phi]$ . Since one knows [9,10] that any local density  $n(\mathbf{r})$  is the equilibrium local density for some potential,  $\phi[n]$ , one can equally well write (allowing for a slight abuse of notation)  $\Omega[n] = \Lambda[n; \phi[n]]$ . But the right-hand side here is  $F[n] + \int n(\mathbf{r})[\phi(\mathbf{r}; [n]) - \mu] d\mathbf{r}$ , so the intrinsic Helmholtz free energy functional can be obtained as

$$F[n] = \Omega[n] - \int n(\mathbf{r})[\phi(\mathbf{r}; [n]) - \mu] d\mathbf{r}. \tag{A4}$$

Using this together with Eqs. (A1)–(A3) gives

$$\beta F[n] = \beta F_{id}[n] + (1 - N[n]) \ln(1 - N[n]) + N[n]. \tag{A5}$$

For a spherical cavity of radius  $R + \varepsilon$  and with zero field inside the cavity, and writing the volume of a  $D$ -dimensional spherical cavity of radius  $R$  as  $V_D(R)$ , Eq. (A2) gives

$$n_\varepsilon(\mathbf{r}) = \frac{\Lambda^{-D} \Theta(\varepsilon - r)}{1 + \Lambda^{-D} V_D(\varepsilon) \exp(-\beta\mu)} = N[n] \frac{\Theta(\varepsilon - r)}{V_D(\varepsilon)}, \tag{A6}$$

which shows that  $\lim_{\varepsilon \rightarrow 0} n_\varepsilon(\mathbf{r}) = N\delta(\mathbf{r})$ . The calculation generalizes trivially for any number of cavities that do not intersect as well as the case that they have a nonzero mutual intersection. For other cases, the results become more complex. For example, for three spherical cavities having the property that  $S_1 \cap S_2 \neq \emptyset \neq S_2 \cap S_3$  but  $S_1 \cap S_3 = \emptyset$ , one finds

$$n(\mathbf{r}) = \left( \frac{x + x^2}{1 + 3x + x^2} \right) V_D^{-1}(\varepsilon) [\Theta(\varepsilon - |\mathbf{r} - \mathbf{S}_1|) + \Theta(\varepsilon - |\mathbf{r} - \mathbf{S}_3|)] + \frac{x}{1 + 3x + x^2} V_D^{-1}(\varepsilon) \Theta(\varepsilon - |\mathbf{r} - \mathbf{S}_2|), \tag{A7}$$

$$x = \frac{3\langle N; [n] \rangle - 3 + \sqrt{5\langle N; [n] \rangle^2 - 10\langle N; [n] \rangle + 9}}{4 - 2\langle N; [n] \rangle},$$

and the Helmholtz free energy functional becomes correspondingly nontrivial.

**APPENDIX B: EVALUATING FMT FOR 0D CAVITIES**

**1. The packing fraction**

Consider a collection of  $m$  0D cavities with centers  $\mathbf{s}_i$ . Note that in the following, everything is written in terms of the limit that the density becomes a sum of  $\delta$  functions, but the same manipulations can be made, more mathematically securely, with cavities slightly larger than a sphere for which the density is not singular (as described in Appendix A) with the same results in the singular limit.

The local density is therefore

$$n(\mathbf{r}) = \sum_{i=1}^m N_i \delta(\mathbf{r} - \mathbf{s}_i), \tag{B1}$$

where the restrictions on the coefficients depend on the geometry: if the cavities are all disjoint, the  $0 \leq N_i \leq 1$ , if there is a nonempty mutual intersection, then  $0 \leq \sum_{i=1}^m N_i \leq N$ , etc. The local packing fraction is

$$\eta(\mathbf{r}) = \sum_{i=1}^m N_i \Theta(R - |\mathbf{r} - \mathbf{s}_i|), \quad (\text{B2})$$

and one verifies that for any function  $\psi(x)$ ,

$$\frac{\partial}{\partial R} \psi[\eta(\mathbf{r})] = \psi'[\eta(\mathbf{r})] \sum_{i=1}^m N_i \delta(R - |\mathbf{r} - \mathbf{s}_i|). \quad (\text{B3})$$

Furthermore, if one writes

$$\eta(\mathbf{r}) = \lim_{R_1 \dots R_m \rightarrow R} \sum_{i=1}^m N_i \Theta(R_i - |\mathbf{r} - \mathbf{s}_i|), \quad (\text{B4})$$

then

$$\begin{aligned} \frac{\partial}{\partial R_i} \psi[\eta(\mathbf{r})] &= \psi'[\eta(\mathbf{r})] N_i \delta(R_i - |\mathbf{r} - \mathbf{s}_i|), \\ \frac{\partial^2}{\partial R_i \partial R_j} \psi[\eta(\mathbf{r})] &= \psi''[\eta(\mathbf{r})] N_i N_j \delta(R_i - |\mathbf{r} - \mathbf{s}_i|) \delta(R_j - |\mathbf{r} - \mathbf{s}_j|) + \delta_{ij} \psi'[\eta(\mathbf{r})] N_i \delta'(R_i - |\mathbf{r} - \mathbf{s}_i|), \end{aligned} \quad (\text{B5})$$

and so forth.

## 2. A lemma

We will also need to evaluate terms of the form

$$\int \psi[\eta(\mathbf{r}; [\rho])] d\mathbf{r}, \quad (\text{B6})$$

which in general will depend on the geometry. To do so, let the volume of the sphere centered at  $\mathbf{s}_i$  and having radius  $R_i$  be  $V_i = V_D(R_i)$ , let the volume of the intersection between spheres  $i$  and  $j$  be  $V_{ij}$ , the mutual intersection of  $i$ ,  $j$  and  $k$  be  $V_{ijk}$ , etc. Finally, let  $\tilde{V}_i$  be the subvolume of cavity  $i$  which is not a simultaneous part of any other cavity,  $\tilde{V}_{ij}$  the subvolume of the intersection of cavities  $i$  and  $j$  which is not in the intersection with any third cavity, etc. For three cavities,

$$\begin{aligned} \tilde{V}_{123} &= V_{123}, \\ \tilde{V}_{12} &= V_{12} - \tilde{V}_{123} = V_{12} - V_{123}, \\ \tilde{V}_1 &= V_1 - \tilde{V}_{12} - \tilde{V}_{13} - \tilde{V}_{123} = V_1 - V_{12} - V_{13} + V_{123}. \end{aligned} \quad (\text{B7})$$

Then, for  $m$  cavities, one has that

$$\int \psi[\eta(\mathbf{r}; [\rho])] d\mathbf{r} = \sum_{i=1}^m \tilde{V}_i \psi(N_i) + \sum_{i<j=1}^m \tilde{V}_{ij} \psi(N_i + N_j) + \sum_{i<j<k=1}^m \tilde{V}_{ijk} \psi(N_i + N_j + N_k) + \dots, \quad (\text{B8})$$

and specializing to  $m = 3$ , this can be written as

$$\begin{aligned} \int \psi[\eta(\mathbf{r}; [\rho])] d\mathbf{r} &= V_{123} \left[ \psi(N_1 + N_2 + N_3) - \sum_{i<j=1}^3 \psi(N_i + N_j) + \sum_{i=1}^3 \psi(N_i) \right] \\ &+ \sum_{i<j=1}^3 V_{ij} [\psi(N_i + N_j) - \psi(N_i) - \psi(N_j)] + \sum_{i=1}^3 V_i \psi(N_i). \end{aligned} \quad (\text{B9})$$

Note that the case  $m = 2$  follows by setting  $V_{123} = V_{13} = V_{23} = 0$  and that of  $m = 1$  is just  $V_1 \psi(N_1)$ .

## 3. Evaluation of $F_{\text{ex}}[n]$

Now, consider the first FMT term,

$$F_{\text{ex}}^{(1)}[\rho] = \int d\mathbf{r} \psi_1[\eta(\mathbf{r}; [\rho])] \int d\mathbf{r}_1 \rho(\mathbf{r} - \mathbf{r}_1) \delta(R - r_1) K_1(\mathbf{r}_1) \quad (\text{B10})$$

$$\begin{aligned}
 &= \int d\mathbf{r} \psi_1[\eta(\mathbf{r}; [\rho])] \sum_{i=1}^m N_i \delta(R - |\mathbf{r} - \mathbf{s}_i|) K_1(\widehat{\mathbf{r}}_i) \\
 &= \bar{K}_1 \frac{\partial}{\partial R} \int d\mathbf{r} \psi_0[\eta(\mathbf{r}; [\rho])]
 \end{aligned}$$

for some function  $\psi_0(x)$  satisfying  $\psi_1(x) = \psi_0'(x)$  and where it is noted that since  $K_1$  is a scalar, it must be a constant. Using Eq. (B9) for the case of  $m = 3$ , this gives

$$\begin{aligned}
 F_{\text{ex}}^{(1)}[\rho] &= \bar{K}_1 \frac{\partial}{\partial R} V_{123} \left[ \psi(N_1 + N_2 + N_3) - \sum_{i<j=1}^3 \psi(N_i + N_j) + \sum_{i=1}^3 \psi(N_i) \right] \\
 &+ \bar{K}_1 \sum_{i<j=1}^3 \frac{\partial}{\partial R} V_{ij} [\psi(N_i + N_j) - \psi(N_i) - \psi(N_j)] \\
 &+ \bar{K}_1 \frac{\partial}{\partial R} V(R) \sum_{i=1}^3 \psi(N_i). \tag{B11}
 \end{aligned}$$

For the two-body contribution, one requires

$$\begin{aligned}
 F_{\text{ex}}^{(2)}[\rho] &= \int d\mathbf{r} \psi_2[\eta(\mathbf{r}; [\rho])] \int d\mathbf{r}_1 d\mathbf{r}_2 \rho(\mathbf{r} - \mathbf{r}_1) \rho(\mathbf{r} - \mathbf{r}_2) \delta(R - r_1) \delta(R - r_2) K_2(\mathbf{r}_1, \mathbf{r}_2) \\
 &= \sum_{i,j=1}^m N_i N_j \int d\mathbf{r} \psi_2[\eta(\mathbf{r}; [\rho])] \delta(R - |\mathbf{r} - \mathbf{s}_i|) \delta(R - |\mathbf{r} - \mathbf{s}_j|) K_2(\mathbf{r} - \mathbf{s}_i, \mathbf{r} - \mathbf{s}_j), \tag{B12}
 \end{aligned}$$

and noting that  $K_2(\mathbf{r}_1, \mathbf{r}_2)$  can only be a function of  $\mathbf{r}_1 \cdot \mathbf{r}_2$  and that in general for any function  $f(x)$

$$\delta(R - r_1) \delta(R - r_2) f(\mathbf{r}_1 \cdot \mathbf{r}_2) = \delta(R - r_1) \delta(R - r_2) f \left[ \frac{r_1^2 + r_2^2 - (\mathbf{r}_1 - \mathbf{r}_2)^2}{2} \right] = \delta(R - r_1) \delta(R - r_2) f \left\{ R^2 \left[ 1 - \frac{(\mathbf{r}_1 - \mathbf{r}_2)^2}{2R^2} \right] \right\}, \tag{B13}$$

so

$$F_{\text{ex}}^{(2)}[\rho] = \sum_{i,j=1}^m \bar{K}_2 \left( 1 - \frac{s_{ij}^2}{2R^2} \right) \int d\mathbf{r} \psi_2[\eta(\mathbf{r}; [\rho])] N_i N_j \delta(R - |\mathbf{r} - \mathbf{s}_i|) \delta(R - |\mathbf{r} - \mathbf{s}_j|) \tag{B14}$$

for some function  $\bar{K}_2(x)$ . Assuming that  $\bar{K}_2(1) = 0$ , as discussed in the main text, this gives

$$F_{\text{ex}}^{(2)}[\rho] = \sum_{i,j=1}^m \bar{K}_2 \left( 1 - \frac{s_{ij}^2}{2R^2} \right) \lim_{R_i, R_j \rightarrow R} \frac{\partial^2}{\partial R_i \partial R_j} \int \psi_0[\eta(\mathbf{r}; [\rho])] d\mathbf{r}. \tag{B15}$$

For  $m = 2$ , this becomes

$$F_{\text{ex}}^{(2)}[\rho] = [\psi(N_1 + N_2) - \psi(N_1) - \psi(N_2)] 2\bar{K}_2 \left( 1 - \frac{s_{12}^2}{2R^2} \right) \lim_{R_1, R_2 \rightarrow R} \frac{\partial^2}{\partial R_1 \partial R_2} V_{12}. \tag{B16}$$

The evaluation of  $F_{\text{ex}}^{(3)}[\rho]$  proceeds similarly.

### APPENDIX C: REPRODUCING THE 1D FUNCTIONAL

In this Appendix, it is shown that as long as the three-body (and higher order) kernels satisfy the stability condition (i.e., they vanish whenever two arguments are the same), they can give no contribution to 1D dimensional crossover and, so, preserve the Percus functional. To see this, consider the  $n$ -body term

$$F_{\text{ex}}^{(n)}[\rho] = \int d\mathbf{r} \psi_n[\eta(\mathbf{r}; [\rho])] \int d\mathbf{r}_1 \cdots d\mathbf{r}_n \rho(\mathbf{r} - \mathbf{r}_1) \cdots \rho(\mathbf{r} - \mathbf{r}_n) \delta(R - r_1) \cdots \delta(R - r_n) K_n(\widehat{\mathbf{r}}_1, \dots, \widehat{\mathbf{r}}_n), \tag{C1}$$

and the restriction of the density to one dimension

$$\rho(\mathbf{r}) = \delta(x) \delta(y) \rho(z) \tag{C2}$$

so that

$$\rho(\mathbf{r} - \mathbf{r}_i) \delta(R - r_i) = \delta(x - x_i) \delta(y - y_i) \rho(z - z_i) \delta(R - \sqrt{x_i^2 + y_i^2 + z_i^2})$$

$$\begin{aligned}
&= \delta(x - x_i)\delta(y - y_i)\rho(z - z_i)\delta(R - \sqrt{x^2 + y^2 + z_i^2}) \\
&= \delta(x - x_i)\delta(y - y_i)\rho(z - z_i) \left[ \frac{R}{|z_i|} \delta(z_i - \sqrt{R^2 - x^2 - y^2}) + \frac{R}{|z_i|} \delta(z_i + \sqrt{R^2 - x^2 - y^2}) \right] \Theta(R^2 - x^2 - y^2) \\
&= \left[ \frac{R}{\sqrt{R^2 - x^2 - y^2}} \rho(z - \sqrt{R^2 - x^2 - y^2}) \Theta(R^2 - x^2 - y^2) \right] \\
&\quad \times \delta(x - x_i)\delta(y - y_i) [\delta(z_i - \sqrt{R^2 - x^2 - y^2}) + \delta(z_i + \sqrt{R^2 - x^2 - y^2})]. \tag{C3}
\end{aligned}$$

This means that the kernel is evaluated with

$$\hat{\mathbf{r}}_i = \frac{\mathbf{r}_i}{R} = \frac{x\hat{\mathbf{x}} + y\hat{\mathbf{y}} \pm \sqrt{R^2 - x^2 - y^2}\hat{\mathbf{z}}}{R} \tag{C4}$$

so that for  $n \geq 3$  it is always the case that at least two are the same and so the kernel vanishes. Thus, these higher-order terms cannot affect the crossover to 1D.

- 
- [1] S. Luukkonen, M. Levesque, L. Belloni, and D. Borgis, Hydration free energies and solvation structures with molecular density functional theory in the hypernetted chain approximation, *J. Chem. Phys.* **152**, 064110 (2020).
- [2] J. F. Lutsko, How crystals form: A theory of nucleation pathways, *Sci. Adv.* **5**, eaav7399 (2019).
- [3] J. Lam and J. F. Lutsko, Lattice induced crystallization of nanodroplets: The role of finite-size effects and substrate properties in controlling polymorphism, *Nanoscale* **10**, 4921 (2018).
- [4] R. Evans, M. C. Stewart, and N. B. Wilding, A unified description of hydrophilic and superhydrophobic surfaces in terms of the wetting and drying transitions of liquids, *Proc. Natl. Acad. Sci. USA* **116**, 23901 (2019).
- [5] J. K. Percus, Equilibrium state of a classical fluid of hard rods in an external field, *J. Stat. Phys.* **15**, 505 (1976).
- [6] J. K. Percus, One-dimensional classical fluid with nearest-neighbor interaction in arbitrary external field, *J. Stat. Phys.* **28**, 67 (1981).
- [7] T. K. Vanderlick, H. T. Davis, and J. K. Percus, The statistical mechanics of inhomogeneous hard rod mixtures, *J. Chem. Phys.* **91**, 7136 (1989).
- [8] Y. Rosenfeld, Free-Energy Model for the Inhomogeneous Hard-Sphere Fluid Mixture and Density-Functional Theory of Freezing, *Phys. Rev. Lett.* **63**, 980 (1989).
- [9] R. Evans, The nature of the liquid-vapour interface and other topics in the statistical mechanics of nonuniform, classical fluids, *Adv. Phys.* **28**, 143 (1979).
- [10] J. F. Lutsko, Recent developments in classical density functional theory, in *Advances in Chemical Physics*, edited by S. A. Rice, Vol. 144 (John Wiley & Sons, Ltd., 2010), Chap. 1, pp. 1–92.
- [11] Y. Rosenfeld, M. Schmidt, H. Löwen, and P. Tarazona, Fundamental-measure free-energy density functional for hard spheres: Dimensional crossover and freezing, *Phys. Rev. E* **55**, 4245 (1997).
- [12] P. Tarazona and Y. Rosenfeld, From zero-dimension cavities to free-energy functionals for hard disks and hard spheres, *Phys. Rev. E* **55**, R4873(R) (1997).
- [13] R. Roth, R. Evans, A. Lang, and G. Kahl, Fundamental measure theory for hard-sphere mixtures revisited: The White Bear version, *J. Phys.: Condens. Matter* **14**, 12063 (2002).
- [14] H. Hansen-Goos and R. Roth, Density functional theory for hard-sphere mixtures: The White Bear version mark II, *J. Phys.: Condens. Matter* **18**, 8413 (2006).
- [15] J. F. Lutsko, Properties of non-fcc hard-sphere solids predicted by density functional theory, *Phys. Rev. E* **74**, 021121 (2006).
- [16] J. F. Lutsko and J. Lam, Classical density functional theory, unconstrained crystallization, and polymorphic behavior, *Phys. Rev. E* **98**, 012604 (2018).
- [17] J. F. Lutsko and C. Schoonen, Classical density-functional theory applied to the solid state, *Phys. Rev. E* **102**, 062136 (2020).
- [18] S. Labík, J. Kolafa, and A. Malijevský, Virial coefficients of hard spheres and hard disks up to the ninth, *Phys. Rev. E* **71**, 021105 (2005).
- [19] J. Kolafa, S. Labík, and A. Malijevský, Accurate equation of state of the hard sphere fluid in stable and metastable regions, *Phys. Chem. Chem. Phys.* **6**, 2335 (2004).
- [20] D. A. Young and B. J. Alder, Studies in molecular dynamics. XIII. Singlet and pair distribution functions for hard-disk and hard-sphere solids, *J. Chem. Phys.* **60**, 1254 (1974).
- [21] R. D. Groot, N. M. Faber, and J. P. van der Eerden, Hard sphere fluids near a hard wall and a hard cylinder, *Mol. Phys.* **62**, 861 (1987).
- [22] A. Fortini and M. Dijkstra, Phase behavior of hard spheres confined between parallel hard plates: Manipulation of colloidal crystal structures by confinement, *J. Phys.: Condens. Matter* **18**, L371 (2006).
- [23] C. H. Bennett and B. J. Alder, Studies in molecular dynamics. IX. Vacancies in hard sphere crystals, *J. Chem. Phys.* **54**, 4796 (1971).
- [24] M. N. Bannerman, L. Lue, and L. V. Woodcock, Thermodynamic pressures for hard spheres and closed-virial equation-of-state, *J. Chem. Phys.* **132**, 084507 (2010).
- [25] M. Oettel, S. Görig, A. Härtel, H. Löwen, M. Radu, and T. Schilling, Free energies, vacancy concentrations, and density distribution anisotropies in hard-sphere crystals: A combined

- density functional and simulation study, *Phys. Rev. E* **82**, 051404 (2010).
- [26] S. K. Kwak, Y. Cahyana, and J. K. Singh, Characterization of mono- and divacancy in FCC and HCP hard-sphere crystals, *J. Chem. Phys.* **128**, 134514 (2008).
- [27] J. F. Lutsko and M. Baus, Nonperturbative density-functional theories of classical nonuniform systems, *Phys. Rev. A* **41**, 6647 (1990).
- [28] P. Tarazona, Density Functional for Hard Sphere Crystals: A Fundamental Measure Approach, *Phys. Rev. Lett.* **84**, 694 (2000).
- [29] V. B. Warshavsky, D. M. Ford, and P. A. Monson, On the mechanical stability of the body-centered cubic phase and the emergence of a metastable ci16 phase in classical hard sphere solids, *J. Chem. Phys.* **148**, 024502 (2018).
- [30] V. B. Warshavsky, P. A. Monson, and D. M. Ford, Density-functional theory study of the body-centered-cubic and ci16 hard-sphere crystals, *J. Chem. Phys.* **150**, 134506 (2019).
- [31] A. Santos, Class of consistent fundamental-measure free energies for hard-sphere mixtures, *Phys. Rev. E* **86**, 040102(R) (2012).